Surface & Coatings Technology 309 (2017) 203–211

Contents lists available at ScienceDirect

Surface & Coatings Technology

journal homepage: www.elsevier.com/locate/surfcoat

Effect of anodizing time on the mechanical properties of porous titania coatings formed by micro-arc oxidation

Emanuel Santos Jr. [a,*], Gelson B. de Souza [b], Francisco C. Serbena [b], Henrique L. Santos [b], Gabriel G. de Lima [c], Eduardo M. Szesz [c], Carlos M. Lepienski [c], Neide K. Kuromoto [c]

[a] Centro Universitário de Volta Redonda (UniFOA), Volta Redonda, RJ, Brazil
[b] Universidade Estadual de Ponta Grossa (UEPG), Dept. of Physics, Laboratory of Mechanical Properties and Surfaces, Ponta Grossa, PR, Brazil
[c] Universidade Federal do Paraná (UFPR), Dept. of Physics, Curitiba, PR, Brazil

ARTICLE INFO

Article history:
Received 21 July 2016
Revised 23 October 2016
Accepted in revised form 16 November 2016
Available online 19 November 2016

Keywords:
Micro-arc oxidation
TiO_2 coating
Residual stress
Mechanical properties
Adhesion
Nanoindentation

ABSTRACT

Porous TiO_2 coatings were produced on commercially pure Ti substrates by micro-arc oxidation (MAO) in 1.0 M H_2SO_4 electrolyte for different anodizing times. Their mechanical properties were assessed by means of instrumented indentation, XRD residual stress measurements and scratch resistance tests. The rutile/anatase ratio increased from ~0 up to 84% in the 10–360 s anodizing time range, with further increase of coating thickness, porosity and roughness. Titania coatings produced for 180 and 360 s had poor adhesion and uneven surfaces with spontaneous detachment from the substrate. Coating hardness ranged from 3.5 up to 4.0 GPa (close to Ti), whereas the effective elastic modulus varied from 110 up to 120 GPa (19% lower than Ti), regardless of the substrate effects. Coatings exhibited tensile residual stresses, while the substrate compressive stress increased forming a plateau at about −110 MPa for anodizing time longer than 60 s. The presence of such hardened layer beneath the interface improved the coating integrity in the scratch tests under the severe tribological condition, thereby increasing about tenfold the detachment critical load for the samples prepared in the 10–60 s MAO time range. Therefore, the 60 s anodizing time can be a useful reference line for producing mechanically resistant porous titania coatings.

1. Introduction

Micro-arc oxidation (MAO) or Plasma Electrolytic Oxidation (PEO) is an ordinary electrochemical technique used to improve the bioactivity of titanium implants by growing a porous TiO_2 coating on their surfaces [1–3]. In this case, the final characteristics of the TiO_2 coatings strongly depend on the processing parameters, such as the electrolyte used, voltage or current density applied, anodizing time and temperature [2,4–6]. The differences in surface morphology and chemistry lead to preparing TiO_2 coatings with distinct properties, mostly presenting favorable bioactive responses. However, in spite of such a rich and important gathering of knowledge that arise every year from biomaterial research community, some aspects of the MAO process still demand the proper parameterization for practical purposes. The mechanical behavior is a right example. Bioactive MAO coatings on pure Ti, presenting additional features for osseointegration, were shown to be brittle under normal loading and detach from substrate under tangential loads as low as 220 mN [7]. In this way, previous studies focused on the parameters for production of MAO coatings, highlighting the mechanical stability of the bioactive coatings to maintain or even to enhance the original surface conditions. Coating adhesion can be improved by a titanium substrate pre-treatment (shot blasting or plasma nitriding, for example), which are responsible for changing the oxide growth kinetics [8,9].

The aim of the present work is to shed light on the anodizing time parameter; herein investigated as a single possible control parameter for both mechanical features and adhesion of the coatings, which are mandatory to the parameterization of bioactive coatings on metal prostheses. MAO coatings were prepared in the 10–360 s anodizing time range, providing different structure and morphology characteristics. Hardness and elastic modulus were assessed by instrumented indentation due to the small layer volume compared to the bulk material [10]. In addition, analytical methods were employed to minimize spurious effects from surface topographies on the indentation results. The coating adhesion was evaluated by means of scratch tests, where surfaces were locally submitted to severe sliding conditions which are generated by high compressive stresses arising from the sharp pyramidal tip. As a matter of fact, little has been investigated about the mechanical properties [11–14], tribological performance [7,8] and film-substrate adhesion of porous titania coatings formed by micro-arc oxidation [6]. Hence, research concerned about the tribo-mechanical and adhesion properties of porous TiO_2 coatings is useful and timely.

* Corresponding author at: Centro Universitário de Volta Redonda, Av. Paulo Erlei Alves Abrantes, 1325, 27240-560 Volta Redonda, RJ, Brazil.
E-mail address: emanuelsantosjr@gmail.com (E. Santos).

http://dx.doi.org/10.1016/j.surfcoat.2016.11.063
0257-8972/

An important correlation between the MAO coating integrity and the anodizing time-dependent microstructure evolution is also found. Such effect is due to both coatings and substrate internal residual stresses, as measured by X-ray diffraction. A close relation between the coating adhesion and the MAO effects on the near surface substrate is established.

2. Experimental

2.1. Sample preparation

Commercially pure Ti (grade 2) sheets with dimensions of 12 × 10 × 0.9 mm were abraded with SiC paper (from 400 to 1200 grits), ultrasonically cleaned in acetone, isopropyl and distilled water, and then dried at 40 °C for 24 h. Micro-arc oxidation (MAO) treatments were carried out by galvanostatic mode in 1.0 M H_2SO_4, 150 mA/cm^2 current density (J) and anodizing time varying from 10 s to 360 s, which formed TiO_2 coatings with different surface morphologies. The electrolyte was stirred at low velocity over the anodizing treatment. Such range was selected according to data from experimental conditions available in the current literature [2–6,15,16]. A platinum sheet was used as a counter-electrode. All coatings presented different grey hues, according to each anodizing time employed.

2.2. Morphology, structure and roughness characterization

The morphologies of the resulting Ti anodic coatings were analyzed by field emission scanning electron microscopy – FEG-SEM (Tescan Mira 3), operating at 20 kV. The crystalline phases were determined by X-ray diffraction with a Rigaku Ultima IV diffractometer, using the Brag-Brentano geometry and CuK$_\alpha$ radiation (λ = 1.54056 Å). The structural changes were analyzed according to powder crystallographic data. Grazing incidence X-ray diffraction was also performed at the incidence angle of 3° in the 2θ ranged from 10° to 60°, with a 0.02° step and 0.5°/min^{-1} velocity.

The average surface roughnesses (R_a) of the coatings were measured by contact profilometry with a Dektak III profilometer. A total of 15 scans were performed to determine the thicknesses, whereas 30 scans with 5.0 mm-length were carried out on each sample for the R_a measurements. Surface porosity and pores diameter were determined by image analysis using the Image Pro Plus® software with SEM images of 6000× and 10,000× magnifications, taken from three different surface regions on the MAO samples.

2.3. Mechanical properties of the coatings

Hardness (H) and elastic modulus (E) were obtained by instrumented indentation technique using a NanoIndenter XP (MTS), following the Oliver-Pharr method [10]. A Berkovich-type diamond tip calibrated with fused-silica sample with known properties (H = 9.5 GPa and E = 73.0 GPa) was employed. Loads varied from 2 to 300 mN in eight successive loading-unloading cycles. A total of 40 indentations were performed on each sample.

In the case of thin coatings, when the indenter tip reaches penetration depths larger than 10% of film thickness, the hardness measurements are considered to be influenced by the substrate. On the other hand, elastic modulus values assessed by indentations through the entire layer region represent actually the coating-substrate composite behavior, since the elastic field under the indenter has a long range, extending into the substrate [17]. The mechanical properties (H and E) of the effective layer can be inferred from instrumented indentation results on the coating-substrate system by means of analytical methods. The effective hardness (H_f) values of TiO_2 layers were calculated by a method described in a previous work [11], which was specifically developed for Ti anodic coatings. The effective elastic modulus (E_f) values of the produced TiO_2 coatings were calculated by the method proposed by Xu and Pharr [18], which modifies the proposal from Gao et al. [19] for its application in varied film-substrate systems. The two methods demand specific information about both coating and substrate, such as the coating thickness (as measured by FEG-SEM cross section analysis), the substrate hardness and elastic modulus (2.3 GPa and 140 GPa, respectively, measured by instrumented indentation), as well as their Poisson's ratio. The Poisson's ratio for Ti is $\nu = 0.32$ [11,12], while for titania coatings is assumed $\nu_r = 0.28$ [11].

Residual stresses at the Ti substrate and the rutile and anatase phases in the anodic coating were measured by X-ray diffraction. A state of biaxial stress ($\sigma_1 = \sigma_2 = \sigma$) was assumed. For the Ti substrate, stresses were calculated by the $\sin^2\psi$ method [20] using the (213) reflection plane from Ti at 139.35° 2θ angle. The ψ angle was varied from 0° to 55° at 5 equally spaced steps in relation to the $\sin^2\psi$ values. The stresses were then calculated according to:

$$\frac{a-a_0}{a_0} = \left(\frac{1+\nu}{E}\right)\sigma\sin^2\psi, \tag{1}$$

where a_0 is the lattice parameter in the stress-free condition assumed to be measured at $\psi = 0$ and a is the difference in the lattice parameter measured at an angle ψ.

The stresses in the rutile and anatase phases in the anodic coatings were determined by the change in the lattice parameters using Rietveld refinement, the GSAS and EXPGUI packages [21]. The X-ray diffractions were taken from 10° to 80° 2θ range in 0.02° steps and with a step scan time from 1 s to 25 s, depending on the sample. The average residual stress was calculated as follows:

$$\overline{\sigma} = -\frac{E_r}{2\nu_p}\cdot\overline{\varepsilon}_p, \tag{2}$$

where E_r and ν_p are the elastic modulus and Poisson's ratio of rutile or anatase, and $\overline{\varepsilon}_p$ is the average strain given by $\Delta V/3V_0$. The applied elastic moduli were 241 GPa and 271 GPa for anatase and rutile, respectively [22]. The Poisson's ratio was considered as 0.28 [11]. ΔV is the unit cell volume difference between the stressed sample and a stress-free reference sample V_0. The stress free reference samples were the anatase powder from Synth (98% purity) and the same anatase powder heat treated at 1100 °C for 16 h in air and then cooled at 5°/min^{-1} to room temperature, turning into rutile phase. This was confirmed by continuous X-ray diffraction at 2°.min^{-1}, as shown in Fig. 1.

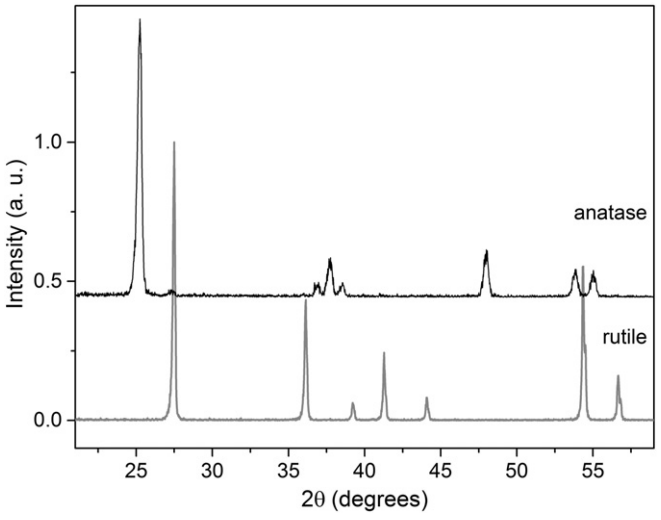

Fig. 1. Continuous X-ray diffraction of the Ti anatase and rutile phases used as stress-free reference samples. The rutile phase was produced by heating the anatase powder at 1100 °C for 16 h in air. Before the heating treatment, the peaks corresponded to the anatase (except the small rutile peak at 27.3°).

2.4. Nanoscratch tests

Scratch tests were performed with the same instrumented indentation facility (the NanoIndenter XP, MTS), following the Berkovich-tip edge direction with scratch velocity of 10 μm/s and 600 μm length. The surface morphology was initially obtained by scanning the track under 50 μN load; then, the tip penetration profile was monitored during loading, and after that, the groove morphology was once again verified (residual depth). Two different loading regimes were employed: (i) from 50 μN to 200 mN (3.3 mN/s loading rate); (ii) from 50 μN to 400 mN (6.7 mN/s loading rate). Additional profiles were obtained by cross-sectioning the grooves at their middle regions (corresponding to 100 or 200 mN applied loads). For each loading condition, the coatings were tested at 3 different spots.

3. Results and discussion

3.1. Morphology and structure

Fig. 2 shows the surface morphologies of the TiO_2 coatings prepared by micro-arc oxidation (MAO). It also displays the voltage-to-time typical curve for galvanostatic MAO process carried out in H_2SO_4 at 150 mA/cm^2. According to previous studies [4], the slope (dV / dt) change at about 100 V denotes the breakdown voltage for the electrolyte (1.0 M H_2SO_4) and current density (150 mA/cm^2) employed herein. From this point on, the observed voltage fluctuation is correlated to the generation of sparks, which turns the oxide outer surface porous with a honeycomb-like appearance. Coatings anodized for 10 s presented pores up to 0.38 μm diameter, while those formed for 60 s had pores with diameter of 0.67 μm at most, as displayed in Table 1. Further, pores became interconnected for longer anodizing time. Such structures could be more favorable to cell adhesion and attachment on bone-anchored dental implants, for example [3]. The coatings produced for 180 s and 360 s disclosed a "layer on layer" like morphology, as seen in Fig. 2. On these surfaces, the pore size increased when the anodizing time did so; however, the layers were loose and easily detached from the 360 s samples. Actually, such feature forbade several measurements to be performed on the 180 s and 360 s samples, as seen in the forthcoming results. Even not being suitable for practical applications, the study of the 180 s and 360 s samples was fortuitous to the understanding of the crystalline structure and the inner stress evolution in the MAO layers.

Fig. 2 also shows representative cross-sectioned regions (in which *layer* and *substrate* are labelled) for all the studied MAO conditions, where the average values are summarized in Table 1. Both coating thickness and surface average roughness R_a parameters increased for

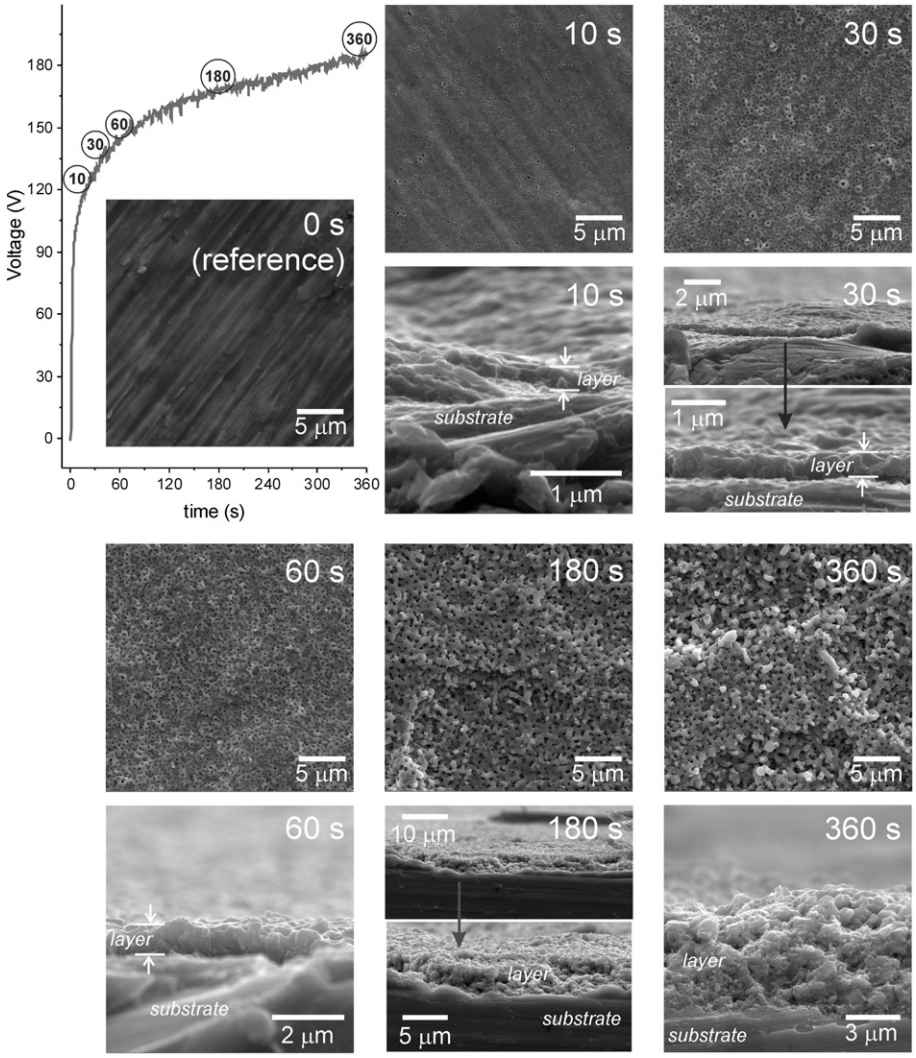

Fig. 2. Typical curve voltage versus time obtained for the micro-arc oxidation process, and representative FEG-SEM images of the titania coatings produced for all the anodizing times. Coatings surfaces were imaged with 5 k× magnification. The cross section images, where *layer* and *substrate* are assigned, allowed to inferring the average coating thicknesses (Table 1). Because of the "layer on layer" like morphology, thicknesses of the 180 s and 360 s samples varied widely through the analyzed coating areas.

Table 1
Morphology parameters and scratch tests results (elastic recovery and critical load) of the MAO porous titania coatings (mean value ± standard deviation).

Sample	Anodizing time (s)	Thickness (μm)[a]	R_a (nm)[b]	Maximum pore diameter (μm)	Surface porosity (%)[c]	Elastic recovery (%)[d]	Critical load for detachment (mN)[e]
cp-Ti	0	–	21 ± 6	–	–	32 ± 4	–
MAO 10	10	0.35 ± 0.10	195 ± 7	0.38	3.2 ± 0.8	60 ± 12	43 ± 5
MAO 30	30	0.61 ± 0.20	225 ± 30	0.42	6.1 ± 1.4	25 ± 6	328 ± 11
MAO 60	60	0.92 ± 0.10	313 ± 60	0.67	9.9 ± 1.4	24 ± 3	≥400
MAO 180[f]	180	≥3	–	–	–	–	–
MAO 360[f]	360	≥4	–	–	–	–	–

[a] n = 8.
[b] n = 30.
[c] n = 3.
[d] at 200 mN load, $n = 3$.
[e] n = 3 (see Fig. 9).
[f] Most tests were not performed on those samples, since they presented a loose character – see text in Section 3.1.

longer anodizing time applied. Such changes were somehow expected, as the coating became thicker with bigger pores and distinct shapes at higher anodic voltages (or longer MAO time). Furthermore, surface porosity also increased for longer anodizing time. Therefore, the increase in the anodizing time might lead to the preparation of adherent coatings, i.e., TiO_2 surfaces that are more suitable to mechanical interlocking in adhesive bonding with bones and cells, for example. Because of the loosening character of the 180 s and 360 s samples, reliable roughness assessments were not possible to be performed. Likewise, their thicknesses varied widely through the coating area, because of these samples superimposed layers feature, as shown in Fig. 2. In such cases, it was possible to infer that the 180 s and 360 s samples were thicker than 3 μm and 4 μm, respectively, being suitable for residual stress measurements, as discussed in Section 3.3.

The evolution of the crystalline structure of the TiO_2 coatings depended on the anodizing time, as shown in Fig. 3. Initially, the TiO_2 coatings were composed of anatase-rich and Ti phases, as observed for 10 s samples. When the anodizing time increased, the rutile structure appeared and grew in contrast to the anatase one, becoming the dominating phase in the samples anodized at longer time. As the anodic voltage raise, the oxide thickness and the effective surface area (followed by pores generation) of TiO_2 coatings did so. The oxide resistance also grows, generating a local heating on the oxide surface [23]. As anatase is a metastable phase, it is transformed into rutile at higher temperatures as the ones found in the electric arc phenomena. The anatase to rutile transformation is a nucleation and growth process [22], therefore, a time-dependent mechanism. Accordingly, samples prepared for 60 s presented a rutile-rich phase in their microstructures, as seen in Fig. 3. At 360 s, the coating is mainly composed of the rutile phase. The Ti peaks from the substrate decreased for longer anodizing times because coatings became thicker.

The aforementioned time-dependent phase evolution is summarized in Fig. 4, which presents the anatase and rutile concentrations in the coatings calculated by Rietveld refinement analyses. For the 30 s anodizing time, the crystal phase composition of the coating is composed of about 2% rutile, which rises almost linearly up to 64% for the 180 s samples. As for the 360 s samples, rutile corresponds to 84% and anatase to 16%. The progressive anatase to rutile transformation is due to the localized temperatures in the 600–700 °C range inside the growing layers [22], possibly running in the micro-arc channels that will eventually originate the typical micro-pores. Such phase transformation and temperature impose stresses and significant changes to the coating mechanical strength, as discussed in Section 3.3.

3.2. Elastic modulus and hardness

Elastic modulus (E) and hardness (H) of the produced TiO_2 coatings were measured by instrumented indentation technique. Because of their poor adhesion and presence of loose plates on the surface, results were not possible to be obtained on the coatings produced for 180 s and 360 s MAO times. To obtain the most accurate values, the measurements must be preferably carried out on flat and smooth surfaces, since the tip-asperity interactions can lead to errors in the "zero" depth determination in the load versus displacement curves. This effect changes the maximum penetration value used in the calculation of the elastic modulus and hardness by the Oliver and Pharr's method [10]. Nevertheless,

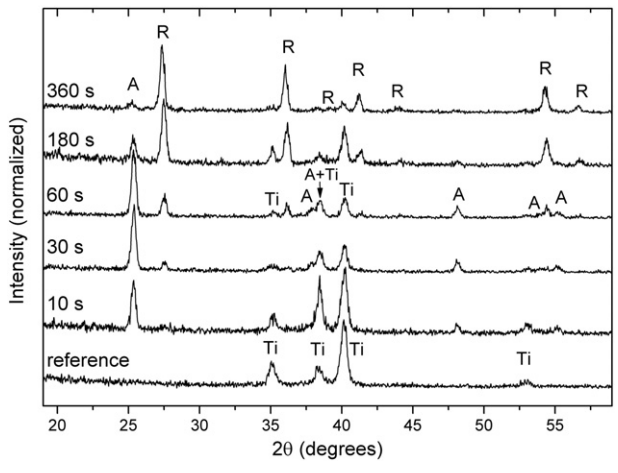

Fig. 3. Grazing X-ray diffraction at 3° of Ti surfaces submitted to different MAO anodizing times. As the time increases, the titania coatings grew, being composed mainly of anatase phase for short time, which transformed to rutile for longer periods. A = anatase, R = rutile, and Ti = titanium.

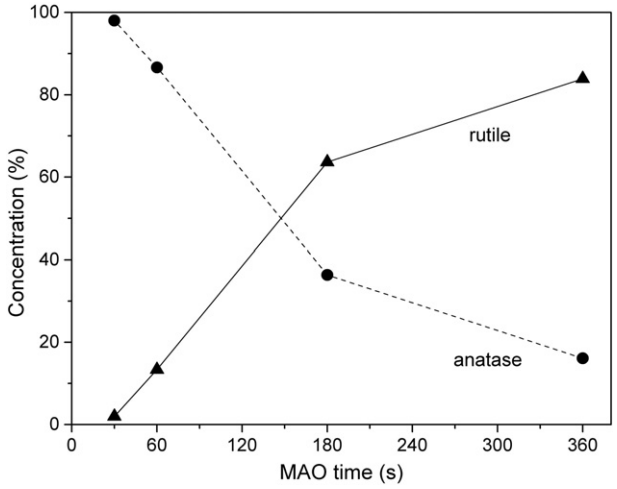

Fig. 4. The anatase and rutile phase concentration in the MAO titania coatings calculated by Rietveld refinements from XRD results. Because of its low concentration, rutile was not possible to be quantified in the coatings anodized for 10 s.

the MAO process makes the surface porous and rough, as seen in Fig. 2. Since the surface roughness interferes in the E and H measurements, data were corrected by using the contact stiffness analysis detailed elsewhere [24]. In this method, the derivative of load with respect to displacement is analyzed to determine the effective point where surface starts to be indented. Hardness and elastic modulus are then recalculated by the usual Oliver and Pharr method [10].

Even so, noticeable standard deviation bars were obtained, which can be mostly attributed to the presence of pores and pore deformation while being loaded, affecting the area calculation. Fig. 5 shows the E values obtained at different contact depths (or loads) for the substrate (cp-Ti) and the Ti oxide coatings prepared for 10, 30 and 60 s. The cp-Ti sample has E of about 140 GPa, being in good agreement with the literature [7,12]. All surfaces, referred as "coating + substrate composites" in Fig. 5 (close symbols), presented lower E values as compared to Ti. Besides, there are no evident or remarkable differences among the E measured for the three types of surfaces. Even at contact depths lower than the coatings thicknesses, the elastic modulus is strongly influenced by the substrate beneath [17]. In Fig. 5, the open symbols refer to the effective elastic modulus (E_f) of the coatings, disregarding the effects of the substrate, calculated by the analytical method previously described. In general, the Ti oxide coatings presented E_f in the 100–120 GPa range. The 19% reduction in the E_f values in relation to the cp-Ti substrate is chiefly due to the coatings porosity [25] and it could be an advantage, once load transference between living tissues and prosthesis is critical at the contact zone, which draw attention to the lowering of E at the TiO_2-covered implant surfaces.

Fig. 6 shows the coating-substrate composite hardness (H) measured on the TiO_2 coatings. Taking into account the obtained value dispersion, the H values are very similar for all coatings. However, they have a different behavior from the E measurements, where the values are lower than the substrate. The difference between the calculated effective coating hardness H_f (see Section 2.3) and their respective measured composite hardness are barely 10% (not shown), falling inside the standard deviation of the H measurements. The plastic deformation zone, which rules the hardness measurements, has a shorter range than the elastic one [17]. Even so, inside the layers (see layer thicknesses in Table 1), hardness profiles are influenced by the substrate underneath and drop accordingly, since all of them laid beyond the "critical" 1/10 of the layer thickness [17]. The profiles are still higher than the substrate at regions deeper than the coating thicknesses because H is a balanced measure of Ti and the layer beneath, that is, the plastic deformation accommodated in each of them. Another effect that occurs in the TiO_2 layers during the tip incursion is the compaction of the porous

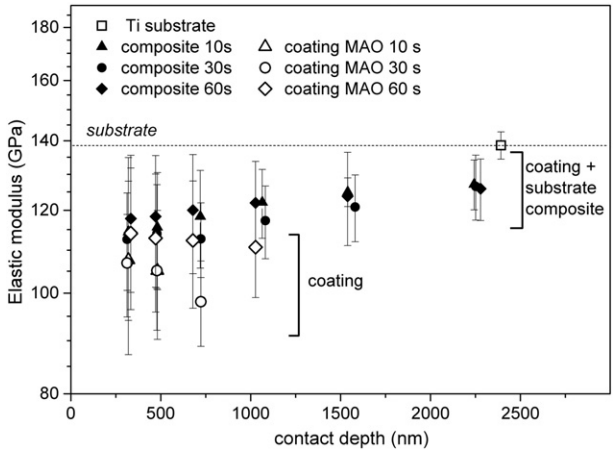

Fig. 5. Elastic modulus (E) of the titania coatings produced by MAO for 10, 30 and 60 s. Close symbols indicate the surface (coating + substrate) results, whereas open symbols correspond to the effective modulus (E_f) of the coatings, regardless of the Ti substrate effects, calculated for depths up to the coating thickness (Table 1) following the method described in Ref. [3].

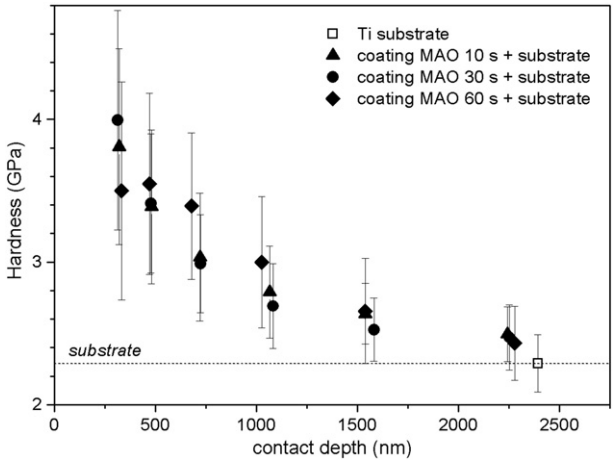

Fig. 6. The composite (coating + substrate) hardness (H) of the titania coatings produced by MAO for 10, 30 and 60 s.

macrostructure, which increases the contact area regardless of the applied ramping load. There are also cracking and fracture events inside the coatings when the indenter load increases. Such brittle behavior has been already observed for Ti anodic layers produced by potentiostatic [12] and galvanostatic [7] modes. The hardness profiles in Fig. 6, in fact, comprise information on the TiO_2 layer microstructure behavior under normal loading, typically featured by pore deformation and microcrack nucleation, as previously reported for porous TiO_2 films [7,12].

In terms of the wear theory, a correlation among coating hardness and elastic modulus with tribological performance can be established [25]. In the present work, however, the measurement of such mechanical properties by indentation tests was strongly affected by the peculiar interconnected porous microstructure. The pore compaction caused by indentation governed the plastic deformation, leading to the decrease of the hardness profiles as seen in Fig. 6; likewise, the elastic modulus is affected by porosity as well, so the values obtained for the produced coatings (Fig. 5) were lower than those for pure bulk titanium dioxides (~270 GPa) [24,26]. To further investigate the effect of the anodizing time on the tribo-mechanical behavior, the residual stresses in the titania coatings were measured and correlated with nanoscratch resistance tests, as follows.

3.3. Residual internal stresses

Fig. 7 shows the residual stresses for Ti substrate and both anatase and rutile phases, present in the MAO coatings, as a function of the anodizing time measured by XRD. The determination of residual stresses for each of the MAO times depended on the adequate intensity of the diffraction peaks (the (213) α-Ti plane for the substrate, and the main anatase and rutile peaks for coatings), as detailed in Section 2.3 and shown in Fig. 3. Thus, for the calculation of the residual stresses, the following hydrogenation times were considered for each phase: 0–180 s for α-Ti; 30–180 s for anatase; 60–360 s for rutile. The Ti substrate stress was compressive, initially increasing when the anodizing time did so. From the 60 s MAO time on, the residual stress was nearly constant at -110 ± 20 MPa. For the anatase phase, the residual stress was tensile and varied from ~720 MPa (30 s sample) to around 520 MPa (180 s sample). A decreasing trend was also observed for the rutile phase, i.e., the tensile residual stress decreased slightly from ~520 MPa (60 s sample) to 390 MPa (360 s sample).

The Ti substrate stress growth indicates that the damage was mainly cumulative when the anodizing time increased. It grew from nearly zero (0 s) to the plateau of about −110 MPa after 60 s anodizing time. As the time raised and the residual stress built up, the value of the Ti yield stress was reached [26]. As the critical resolved shear stress for plastic

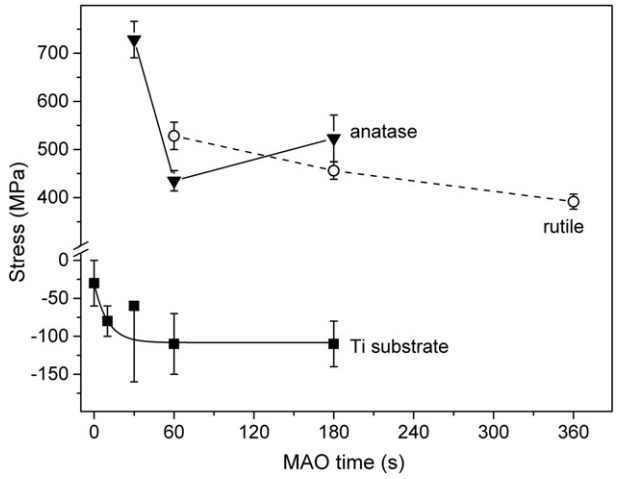

Fig. 7. Residual stresses as a function of the MAO time for Ti substrate, anatase and rutile phases in the titania coatings. The lines are only guides to the eyes.

deformation was attained, the plateau in Fig. 7 took place because any Ti substrate residual stress growth was prevented by the plastic deformation increase. It was reported that the critical resolved shear stress for Ti grade 2 is about 135 MPa [27] with a little work hardening [13], which is in good agreement with the present findings.

Both anatase and rutile phases presented the tensile stress and remained somehow constant for MAO times longer than 60 s. It is worth noting that the coating residual stresses are also influenced by the thermal expansion and elastic mismatches in the coating-substrate interface. Assuming the state of biaxial stress, the residual stress σ_R due to thermal expansion and elastic mismatches can be calculated from [28]:

$$\sigma_R = \frac{E_p}{(1-\nu_p)}\Delta\alpha \cdot \Delta T \tag{3}$$

where E_p and ν_p are the elastic modulus and the Poisson's ratio of coating, respectively. The relation $\Delta\alpha = \alpha_p - \alpha_s$ is the difference between the thermal expansion of the coating (α_p) and the substrate (α_s). ΔT is the temperature difference between the anodizing temperature and the room temperature. The MAO experiments were set up at room temperature. However, as discussed in Section 3.1, dielectric arcs produce intense inner heating in the TiO_2 layers, thereby enabling the anatase to rutile transformation. Thus, the temperature at which such allotropic change begins (600 °C [22]) can be reasonably assumed as the anodizing temperature. Considering the average linear thermal expansion of $5.8 \times 10^{-6}\ K^{-1}$ (anatase), $7.8 \times 10^{-6}\ K^{-1}$ (rutile) [29] and $9.2 \times 10^{-6}\ K^{-1}$ (titanium) [30], residual internal stresses of about −660 MPa and −305 MPa were obtained for the coatings composed solely of anatase and rutile, respectively.

The predicted residual stresses are tensile while the experimental ones are compressive strains. This means that residual stress predictions are only based on the thermal expansion mismatch between the coating and the substrate is not entirely valid. It might be caused by any residual stress built up in the coating prevented by plastic deformation in the substrate while cooling from the high anodizing temperature. As plastic deformation induces compressive stresses in the Ti substrate, there should be a tensile stress in the coating by the equilibrium of forces given by Newton's third law. Different values of residual stresses may arise due to the variation of both anatase/rutile rate and coating porosity obtained at longer anodizing time (see Fig. 4). Other features that affect residual stresses are the anatase to rutile conversion in the coating and its delamination (detachment) as well. The anatase to rutile transformation implies a volume contraction of around 9% due to the density variation, namely: 3.89 g/cm^3 (anatase) and 4.25 g/cm^3 (rutile) [24]. As a matter of fact, such difference promotes a tensile residual stress in the coatings.

On the other hand, the coating delamination relieved stresses for anodizing time longer than 180 s. Hutchinson and Suo [28] have estimated the critical layer thickness h for debonding. Accordingly, the critical thickness to detachment initiation is given by:

$$h = \frac{EG}{Z\sigma^2} \tag{4}$$

where $G = (1-\nu_p^2)$. K_{IC}/E_p is the layer released energy rate, K_{IC} is the stress intensity factor, σ is the experimental residual stress measured by XRD, and Z is a dimensionless constant equal to 1.028. Assuming $K_{IC} = 3.2\ MPa \cdot m^{1/2}$ [31] and $\sigma = 450$ MPa for anatase and rutile phases, the critical layer thickness of about 45 μm for both anatase and rutile was obtained. This means that the anatase to rutile transformation did not contribute for debonding in opposition to the film thickness given by the MAO time, which influenced the results. Because of the inherent porosity found in the MAO coatings, the critical thicknesses for detachment are expected to be lower than the calculated one, as measured herein (Table 1).

3.4. Nanoscratch resistance

Fig. 8 illustrates typical scratch profiles during and after applying the ramping loads from 0.05 mN up to 200 mN, as well as the corresponding FEG-SEM images of the test grooves produced on the samples surfaces. Tests were carried out only on mechanically stable layers which did not present loose layers, that is, the 10 s, 30 s and 60 s samples. The scratch morphology of the Ti substrate (not shown) had a typical ductile behavior [25], being in accordance with previous reports [7]. Scratches on the Ti substrate formed a pile-up at the track edges without the presence of released debris, as well as inner scars following the tip movement, which were produced by ploughing and third-body interaction with the compacted material.

The scratch profiles of the anodic coatings (Fig. 8a–c) revealed that the maximum depths were around 1.5 μm for both 10 s and 30 s samples and about 2.0 μm for the 60 s samples. In addition, the elastic recovery after the load relief was around 60% for 10 s sample and nearly 25% for both 30 s and 60 s samples (see Table 1). In spite of the maximum depths being deeper than the oxides thicknesses (<1 μm), the scratch morphologies were quite different among the three anodizing times. Fig. 8a (10 s sample) shows that, under 100 mN load (see the region labelled as 1), the groove presented substrate-like inner scars produced by plastic plough. In region 2 (around 150 mN load), the material dragged from the preceding regions was lying inside the groove, abraded and compacted by the moving tip, as suggested by the presence of perpendicular cracks observed inside it. In region 3, the typical titanium ductile features predominated, without evidences of the porous coating inside the groove. The debris formed close to the groove edges suggest the occurrence of brittle deformation mechanisms [25], where material from the TiO_2 coating was removed by fracture and deposited perpendicularly on the tip track. The observed elastic recovery for the 10 s samples surface, which is greater than for the substrate (Table 1), might be due to the presence of removed and compacted materials that were formed during the tip sliding and were loosely attached to the substrate. It is worth mentioning that the residual profile was recorded with much smaller tangential load (50 μN) than that obtained during loading.

Differently, the 30 s samples in Fig. 8b retained some porous features of the pristine TiO_2 coating along the groove length (regions 1–3). Nevertheless, the layer morphology was notably changed. The layer was compacted and fractured by scratching (region 2), similarly but less pronounced than the observed for the 10 s samples. So, the substrate was not completely exposed at the end of the scratches (region 3). Even though, tiny pores inside the grooves are also indicative of a high compaction taking place under the 200 mN scratching load. Some

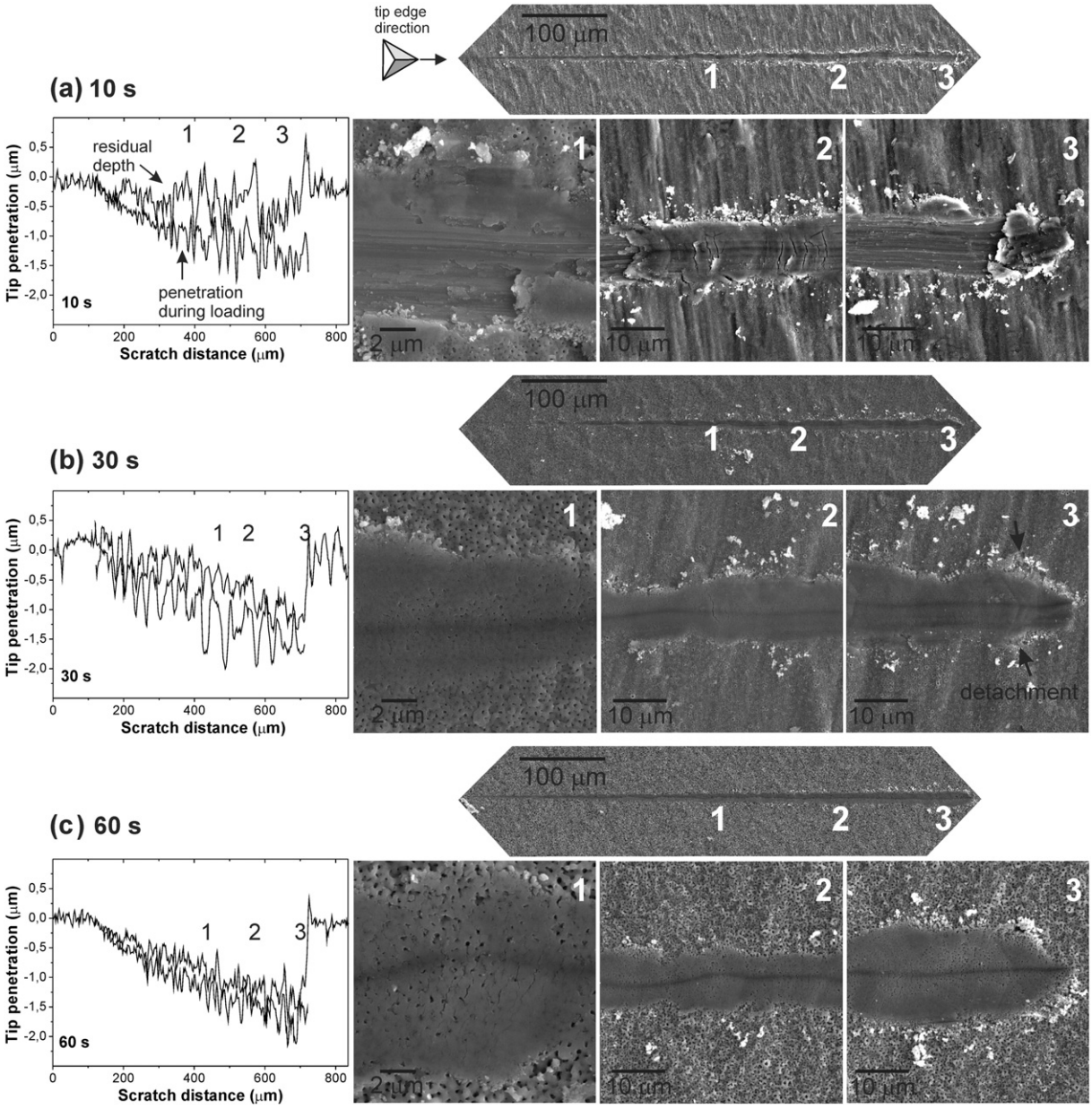

Fig. 8. Scratch tests performed with the Berkovich tip following the tip edge direction under ramping load from 50 μN to 200 mN for samples prepared in the indicated MAO times. The profiles correspond to the penetration during loading and the recorded residual depth. Secondary-electron FEG-SEM images show the entire scratch grooves and magnified areas corresponding to the labels 1, 2 and 3.

layer detachment was observed at the groove edges, as indicated by the arrows. In Fig. 8c, the surface anodized for 60 s had a significant scratch resistance improvement, as compared to the 10 and 30 s anodizing conditions. The released debris and changes in the surface morphology were less pronounced, since the TiO_2 layer retained much of its integrity through the entire scratch length. Accordingly, the track profiles during and after loading were smoother for the 60 s samples compared to the other samples. Moreover, surface detachment after the scratch tests was not observed for such anodizing time.

Additionally, to investigate the scratch mechanisms on the TiO_2 coatings, further tests with loads up to 400 mN were carried out, as seen in Fig. 9. Under such tests conditions, the loading rate was 2-fold higher than the previous tests with 200 mN loads. The 400 mN load tests were aimed at verifying possible changes in the deformation response due to time-dependent plastic effects, which occurs in such small volumes at nm-μm scales [10,25,32,33]. In the present study, the inner pore compaction might contribute to this phenomenon. The regions labelled as 1 in Fig. 9 (at about 200 mN applied load) also include the corresponding cross-section profiles. The groove depths were about 1.0 μm for the 10 s and 30 s samples and 1.2 μm for the 60 s samples; therefore, they were similar to the residual depths observed for the same load under slower sliding tip (Fig. 8). The 10 s samples (Fig. 9a) had similar features as previously observed in Fig. 8a; that is, a plenty of amorphisized material inside the grooves, formation of wear debris and coating detachment at the track edges. The material remaining inside the track, seen in the regions 1 and 2, did not keep the original titania coating morphology. The 30 s and 60 s samples also presented debris releasing and some detachment took place around the scratch grooves; however, contrarily from the 10 s samples, compacted pores from the coating could be observed along the entire groove. Indeed, material compaction and loosening were more severe for the 30 s samples (Fig. 9b) than for the 60 s samples (Fig. 9c), as well as inner crack formation. In addition, no striking differences were observed between the two loading rates, since the scratch morphologies were very similar for the 200 and 400 mN loads.

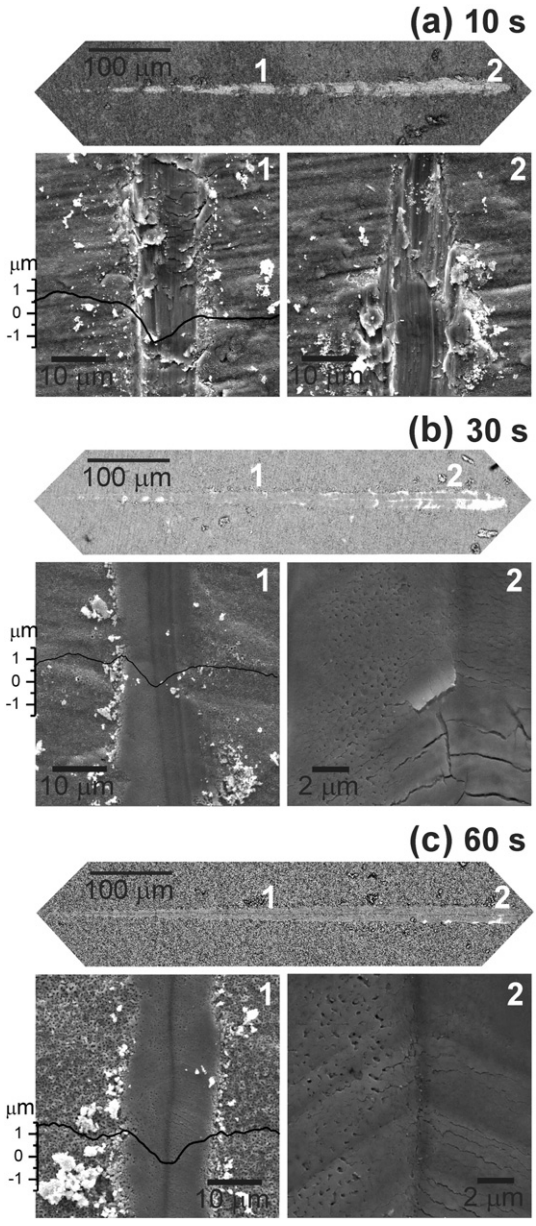

Fig. 9. Scratch tests performed with the Berkovich tip following the tip edge direction under ramping load from 50 μN to 400 mN for samples prepared in the indicated MAO times. The backscattered-SEM images show entire scratch grooves and the secondary-electron FEG-SEM images depict selected areas, labelled as 1 and 2. The corresponding cross-section profiles as obtained at the scratches middle region are shown for comparison purposes.

Critical loads calculated from scratch tests correspond to those load values where notable detachment takes place and the substrate is exposed [25]. They were inferred by a careful groove analysis using the backscattered-SEM images, as depicted in Fig. 9. The obtained values are summarized in Table 1. Even restricted by the loading range of the scratch equipment (40 mN at most), it was found that the critical loads increased one order of magnitude when the anodizing time was changed from 10 s to 60 s.

Therefore, the scratch results clearly indicate an anodizing time dependence upon the tribological behavior of porous titania coatings. It is noteworthy that the nanoscratch tests are particularly suitable to obtain specific responses from coatings. For normal loadings, as those imposed in the nanoindentation tests, the plastic deformation field reaches the substrate for penetrations deeper than ~100 nm (10% of the layer thickness, see Table 1) [17]. On the other hand, the stress distribution in scratch tests also comprises tangential forces due to the moving tip, constraining the plastic deformation in the regions surrounding the stylus tip [34]. Despite the maximum scratch depths being higher than the layer thicknesses, the results disclosed the responses related to the inherent properties of the titania coatings and/or the interface bonding to the Ti substrate. The enhanced coating-substrate adhesion observed in scratch tests is correlated with the residual stress measurements, as discussed next.

4. Final remarks

The growing TiO_2 coating eventually detaches from the Ti substrate, as predicted by Eq. (4) and experimentally observed for the longer MAO times of 180 s and 360 s. It was found that the anatase to rutile ratio had little influence on the critical thickness for coating detachment, as discussed in Section 3.3 and, therefore, to the coating integrity in the scratch tests. On the other hand, the TiO_2 coatings had a notable adhesion enhancement for MAO times from 10 up to 60 s (Table 1).

Thin layer adhesion is strongly connected with two sorts of stresses, namely, the residual internal stresses and those applied in the service [34]. Some authors [14,35,36] have reported that porous TiO_2 coatings grown in the rupture regime of the oxidation process (as the present samples, Fig. 2) had *compressive* stresses. At a first glance, this line of reasoning could explain the adhesion time-dependent phenomenon. Following the model proposed by Choi et al. [35] for titanium oxides produced by MAO, the first stage comprises the oxide thickness growth by increasing anodizing voltage; afterwards, pores are generated by the oxide film electric breakdown. Re-passivation occurs inside the pores, which are submitted to a new breakdown, thereby producing inner pores in other ones previously formed. Arc discharges generate local heating, leading to the gradual anatase to rutile microstructure transformation [22,23,36]. Since rutile has a more compact structure than anatase [22], the concomitant increase in the compressive stresses could contribute to prevent crack initiation and propagation in the coating [25].

In the present work, a different approach is required to account the *tensile* stresses (Fig. 7), instead of the compressive ones, calculated for the MAO layers in the analyzed anodizing time range. Competitive effects including the material densification (due to the TiO_2 allotropic transformation), stress effects in the substrate and the pore settlement after cooling probably took place, regardless of the anatase to rutile ratio. Thus, the resulting coating stresses were tensile ones, balancing the compressive stresses underneath the coating-substrate interfaces. As shown in Fig. 7, such substrate residual stresses increased from −30 to −110 MPa for the 10 s – 60 s anodizing time range. Such case-hardened surface layer on the Ti substrate opposed the additional and external tensile stresses imposed by the scratching tip, thereby allowing the anodic layer to deform with limited presence of cracks. Differently, for longer anodizing times, the substrate inner stress increase was prevented by plastic flows, whereas the critical thickness for detachment was reached, as previously discussed in Section 3.3.

Based on the findings obtained for the porous MAO coatings and the discussion above, it is possible to assert that the 60 s growing time should be considered as a reference line for the production of mechanically resistant porous titania coatings.

5. Conclusions

In the present work, the influence of the anodizing time on the mechanical properties and scratch resistance of porous TiO_2 coatings prepared by micro-arc oxidation in H_2SO_4 electrolyte was studied.

The allotropic transformation of TiO_2, a temperature and time-regulated phenomenon, changed the rutile to anatase ratio from ~0 to 84% when the anodizing time was changed from 10 to 360 s. The surface morphology features were time dependent as well; however, coatings

prepared for 180 s and 360 s spontaneously detached from the Ti substrate.

Hardness values of the MAO coatings (3.5–4.0 GPa) were similar to the Ti substrate. Contrarily, the effective elastic modulus (calculated apart from the substrate) was found in the 110–120 GPa range, that is, around 19% lower than for Ti due to the coating porosity.

The MAO porous coatings had tensile residual stresses for all the anodizing conditions. Such finding could be correlated with the plastic deformation limiting effect in the substrate, which ruled the stress balance between the coating and substrate during cooling. The substrate compressive residual stresses varied from −30 to −110 MPa for the 10 s–60 s anodizing time range, reaching a plateau from longer times.

The tribological behavior was drastically improved among the different scratch test conditions, regardless of the loading rate. The critical loads for the layer integrity as obtained from scratch tests increased about 10-fold when the anodizing time varied from 10 to 60 s. Such effect was due to the enhanced load bearing capacity provided by the case of hardened Ti layer beneath the TiO_2 interface, which was more evident when the rutile-anatase rate increased.

The 60 s anodizing time is the most suitable as a reference line for mechanically resistant titania coatings on Ti for the MAO conditions employed.

Acknowledgements

The authors thank the C-LABMU/UEPG for the FEG and XRD facilities. This work was partially supported by Coordenação de Aperfeiçoamento de Pessoal de Nível Superior, Conselho Nacional de Desenvolvimento Científico e Tecnológico and Fundação Araucária (grant numbers 363/2012, 608/2014) Brazilian funding agencies.

References

[1] T. Kokubo, H. Kim, M. Kawashita, et al., Bioactive metals: preparation and properties, J. Mater. Sci. Mater. Med. 15 (2004) 99–107.
[2] B. Yang, M. Uchida, H.M. Kim, et al., Preparation of bioactive titanium metal via anodic oxidation treatment, Biomaterials 25 (2004) 1003–1010.
[3] L.H. Li, Y.M. Kong, H.M. Kim, et al., Improved biological performance of Ti implants due to surface modification by micro-arc oxidation, Biomaterials 25 (2004) 2867–2875.
[4] Y.T. Sul, C.B. Johansson, Y. Jeong, et al., The electrochemical oxide growth behaviour on titanium in acid and alkaline electrolytes, Med. Eng. Phys. 23 (2001) 329–346.
[5] R. Wilks, E. Santos Jr., E.Z. Kurmaev, et al., Characterization of oxide layers formed on electrochemically treated Ti by using soft X-ray absorption measurements, J. Electron Spectrosc. Relat. Phenom. 196 (2009) 45–50.
[6] J.F. Vanhumbeeck, J. Proost, Current understanding of Ti anodisation: functional, morphological, chemical and mechanical aspects, Corros. Rev. 27 (2009) 117–204.
[7] G.B. de Souza, G.G. de Lima, N.K. Kuromoto, et al., Tribo-mechanical characterization of rough, porous and bioactive Ti anodic layers, J. Mech. Behav. Biomed. Mater. 4 (2011) 796–806.
[8] E.M. Szesz, G.B. de Souza, G.G. de Lima, et al., Improved tribo-mechanical behavior of CaP-containing TiO_2 layers produced on titanium by shot blasting and micro-arc oxidation, J. Mater. Sci. Mater. Med. 25 (2014) 2265–2275.
[9] G.B. de Souza, B.A. da Silva, G. Steudel, et al., Structural and tribo-mechanical characterization of nitrogen plasma treated titanium for bone implants, Surf. Coat. Technol. 256 (2014) 30–36.
[10] W.C. Oliver, G.M. Pharr, An improved technique for determining hardness and elastic-modulus using load and displacement sensing indentation experiments, J. Mater. Res. 7 (1992) 1564–1583.
[11] P. Soares, A. Mikowski, C.M. Lepienski, et al., Hardness and elastic modulus of TiO_2 anodic films measured by instrumented indentation, J. Biomed. Mater. Res. B Appl. Biomater. 4B (2008) 524–530.
[12] E. Santos Jr., N.K. Kuromoto, G.A. Soares, Mechanical properties of titania films used as biomaterials, Mater. Chem. Phys. 102 (2007) 92–97.
[13] A.A. Mendes Filho, C.A. Rovere, S.E. Kuri, et al., A general study of commercially pure Ti subjected to severe plastic deformation: microstructure, strength and corrosion resistance, Matéria (Rio J.) 15 (2010) 254–259.
[14] P. Huang, F. Wang, K. Xu, Y. Han, Mechanical properties of titania prepared by plasma electrolytic oxidation at different voltages, Surf. Coat. Technol. 201 (2007) 5168–5171.
[15] D. Wei, Y. Zhou, D. Jia, et al., Biomimetic apatite deposited on microarc oxidized anatase-based ceramic coating, Ceram. Int. 34 (2008) 1139–1144.
[16] M.V. Diamanti, M. Ormellese, E. Marin, et al., Anodic titanium oxide as immobilized photocatalyst in UV or visible light devices, J. Hazard. Mater. 186 (2011) 2103–2109.
[17] R. Saha, W.D. Nix, Effects of the substrate on the determination of thin film mechanical properties by nanoindentation, Acta Mater. 50 (2002) 23–38.
[18] H. Xu, G.M. Pharr, An improved relation for the effective elastic compliance of a film/substrate system during indentation by a flat cylindrical punch, Scr. Mater. 55 (2006) 315–318.
[19] H. Gao, C.H. Chiu, J. Lee, Elastic contact versus indentation modeling of multilayered materials, Int. J. Solids Struct. 29 (1992) 2471–2492.
[20] I. Noyan, T. Huang, B. York, Residual stress/strain analysis in thin films by X-ray diffraction, Crit. Rev. Solid State Mater. Sci. 20 (1995) 125–177.
[21] A.C. Larson, R.B. Von Dreele, General Structure Analysis System (GSAS), Los Alamos National Laboratory Report LAUR 2000, pp. 86–748.
[22] D.A.H. Hanaor, C.C. Sorrell, Review of the anatase to rutile phase transformation, J. Mater. Sci. 46 (2011) 855–874.
[23] M.R. Bayati, R. Molaei, A. Kajbafvala, et al., Investigation on hydrophilicity of micro-arc oxidized TiO_2 nano/micro-porous layers, Electrochim. Acta 55 (2010) 5786–5792.
[24] G.B. de Souza, A. Mikowski, C.M. Lepienski, et al., Indentation hardness of rough surfaces produced by plasma-based ion implantation processes, Surf. Coat. Technol. 204 (2010) 3013–3017.
[25] B. Bhushan, Nanomechanical Properties of Solid Surfaces and Thin Films, Handbook of Micro/Nano Tribology, CRC Press, Boca Ratón, 1999.
[26] M.A. Meyers, K.K. Chawla, Mechanical Behavior of Materials, Prentice Hall, New Jersey, 1999.
[27] M. Niinomi, Mechanical properties of biomedical titanium alloys, Mater. Sci. Eng. A 243 (1998) 231–236.
[28] J.W. Hutchinson, Z. Suo, in: J.W. Hutchinson, T.Y. Wu (Eds.), Mixed Mode Cracking in Layered Materials, Elsevier, 1991 (http://www.sciencedirect.com/science/article/pii/S0065215608701649.).
[29] D.R. Hummer, P.J. Heaney, J.E. Post, Thermal expansion of anatase and rutile between 300 and 575 K using synchrotron powder X-ray diffraction, Powder Diffract. 22 (2007) 352–357, http://dx.doi.org/10.1154/1.2790965.
[30] P. Hidnert, Thermal expansion of titanium, J. Res. Natl. Bur. Stand. 30 (1943) 101–105.
[31] AZoM, Titanium dioxide - titania (TiO_2) technical notesavailable online at http://www.azom.com/article.aspx?ArticleID=1179 (last accessed on 07.13.2016).
[32] H. Matsukawa, H. Fukuyama, Theoretical study of friction: one-dimensional clean surfaces, Phys. Rev. B 49 (1994) 17286–17292.
[33] K.B. Yoder, Y. Katz, W.W. Gerberich, et al., Deformation rate effect and near surface damage evolution – a nanomechanical probing study, Struct. Mater. 11 (2002) 417–426.
[34] A.C. Fischer-Cripps, Nanoindentation, Springer-Verlag, New York, 2004.
[35] J. Choi, R.B. Wehrspohn, J. Lee, U. Gosele, Anodization of nanoimprinted titanium: a comparison with formation of porous alumina, Electrochim. Acta 49 (2004) 2645–2652.
[36] G. He, L. Xie, Y.F. Yin, et al., Synthesis and mechanism of (101)-preferred orientation rutile titania via anodic spark oxidation, Surf. Coat. Technol. 228 (2013) 201–208.